Proceedings of ISINN-29, JINR, E3-2023-58, Dubna, 2023, p.263 –271

Status and Prospect of Studies of (γ, f) Reaction at MT-25 Microtron

D.V. Kamanin[1], Yu.V. Pyatkov[2,1], A.N. Solodov[1], V.E. Zhuchko[1], Z.I. Goryainova[1], E.A. Kuznetsova[1], O.V. Strekalovsky[1], A.O. Zhukova[1]

[1]*Joint Institute for Nuclear Research, Dubna, Russia*
[2]*National Nuclear Research University MEPhI (Moscow Engineering Physics Institute), Moscow, Russia*

INTRODUCTION

Before to attack the main topic, namely, (γ, *f*) reactions, it is necessary to recall some our previous results. The black plot in figure 1(a) is the fragments mass correlation distribution measured at the two-armed time-of-flight COMETA spectrometer. The projection onto the vertical axis (figure 1(b)) shows the peaks that are centered on the masses 68, 69 ,72 associated with the magic isotopes of Ni. The last peak at the mass 74 is likely corresponds to the semi-magic Cupper nucleus with the charge 29. These peaks were observed earlier in our experiments at the 4π -FOBOS spectrometer and the corresponding pictures are shown in figures 1(c, d). It is clearly seen that only in one spectrometer arm, facing the backing of the Cf source there is a broad peak - which was called Ni-bump.

Another structure so called "rhombic meander" is marked in figure 1(a) by the thick arrow. It consists of the lines were $M_1 + M_2 = \text{const}$ and $M_1 - M_2 = \text{const}$. Figure 1(e) shows schematically the prescission configuration for one specific partition in the Ni-bump. Ni & Sn FFs were really detected in the *opposite arms* due to the break-up of the light FF in the source backing.

The second result also needs to be cited to understand what is observed in the (γ, *f*) reactions. The experiment was performed using a two-armed LIS spectrometer presented in figure 2(a).

The essence of the experiment was that the mass of the fragment was measured ("balanced") twice namely before and after it passes the degrader-foil in the timing detector TD1. Event by event the "initial" mass M_{tt} was measured using the TOF–TOF (time-of-flight–time-of-flight) method (see figure 2(a)) while the TOF–*E* (time-of-flight–energy) method was applied to measure the "resultant" mass M_{te}. The results are presented in figures 2(b, c).

The obvious expectation was that we would see just the usual line M_{tt}, accurate to evaporated neutrons, equal to M_{te}. However, it turned out that a much more complex and physically interesting structure is observed. For instance, the mass M_{tt} of the initial fragment was 140, but due to the break-up in the foil, its mass became predominantly 128. A projection of the two-dimensional distribution onto the *Y* axis is shown in figure 2(b). For comparison, the spectrum from binary fission is presented in grey. The difference is obvious mainly due to the intense peaks of masses 128 u and 134 u associated with the magic isotopes of ^{128}Sn and ^{134}Te.

Bearing in mind that the fusion-fission reaction is out ruled a break-up of the fragment due to inelastic Coulomb scattering in the foil is decisive for the effect observed. In its turn it is possible if the fragment was in the shape isomer state before passing the foil. A mean flight

time between the Cf source and the foil let us to obtain the lower estimate of the shape isomer state life time to be more than 15 ns. This is a mean flight-time for the FF at the base between Cf source and TD1 detector with the Cupper degrader inside.

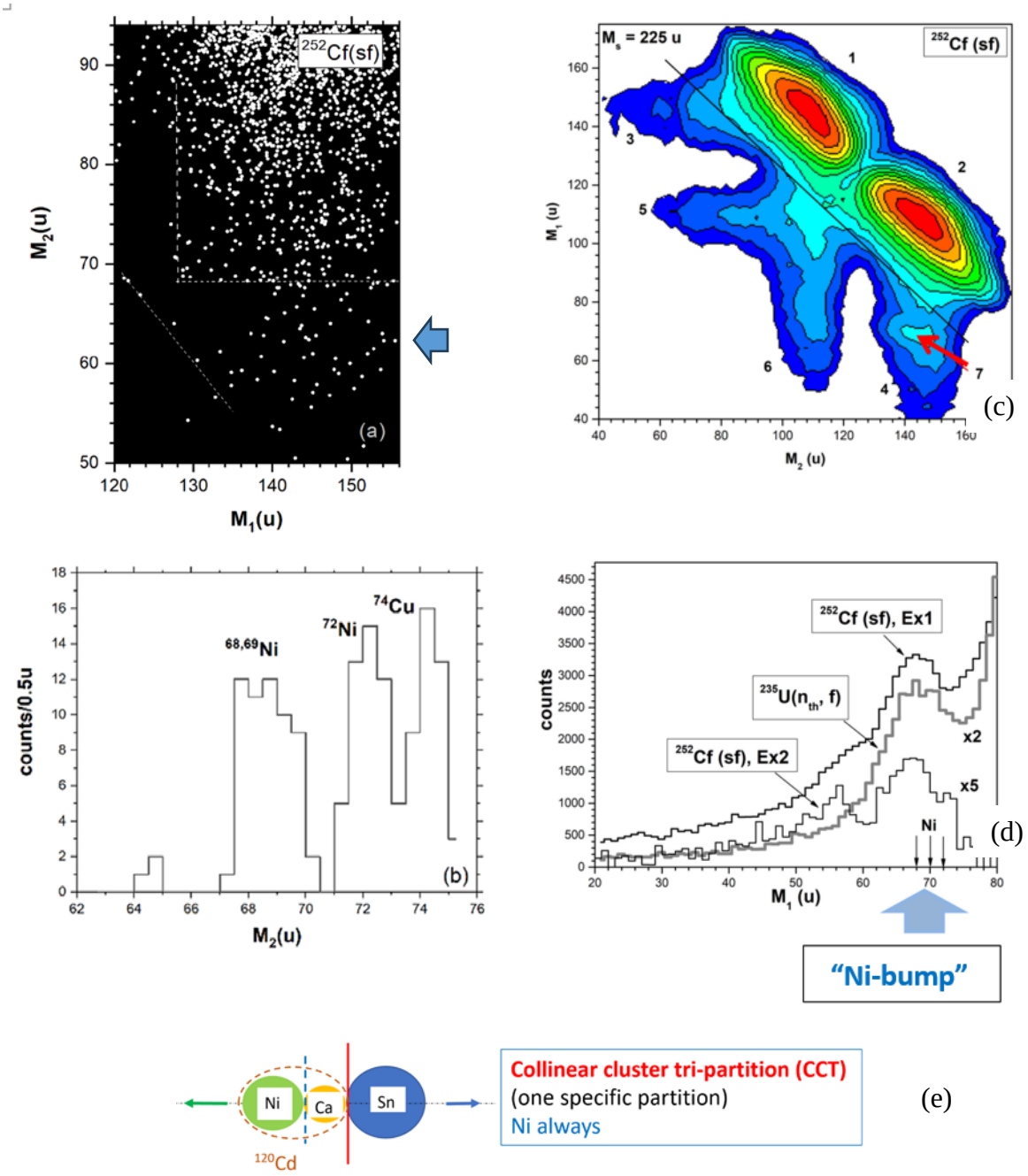

FIGURE 1. FFs mass correlation distribution from ^{252}Cf (sf) (a). Projection of the distribution onto M_1 axis under condition that M_2 = (65 – 76) u – (b). These figures were published in Ref. [1]. Contour map in logarithmic scale of the mass-mass distribution of the collinear fragments of ^{252}Cf (sf), detected in coincidence in the two opposite arms of the FOBOS spectrometer. The arrow marks a specific bump in arm1. (c) Projection of the Ni bump onto M_1 axis obtained in three different experiments performed at the FOBOS spectrometer modules (d). The figures were published in Refs. [2, 3]. Prescission configuration for one specific partition in the Ni-bump (e).

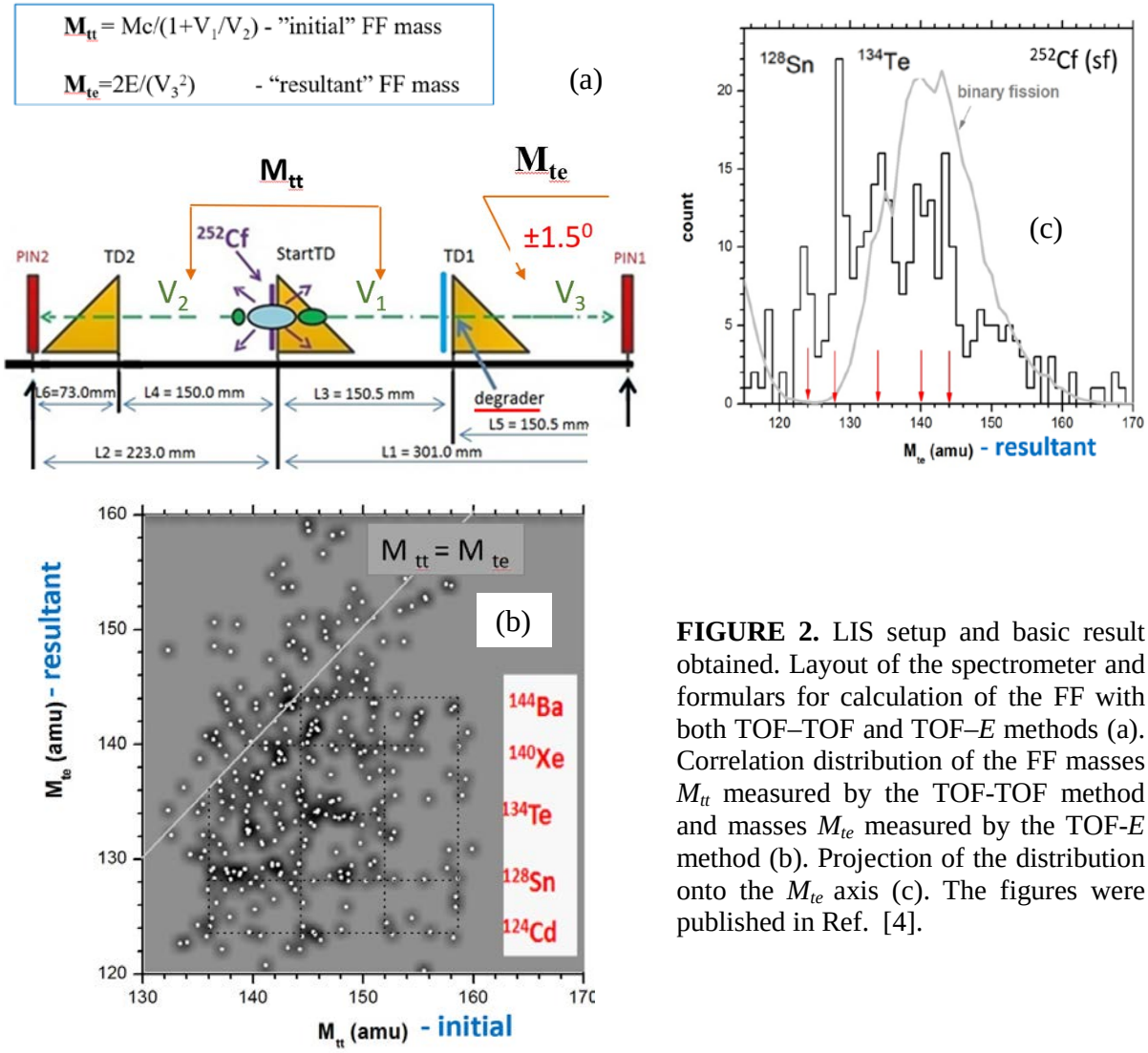

FIGURE 2. LIS setup and basic result obtained. Layout of the spectrometer and formulars for calculation of the FF with both TOF–TOF and TOF–*E* methods (a). Correlation distribution of the FF masses M_{tt} measured by the TOF-TOF method and masses M_{te} measured by the TOF-*E* method (b). Projection of the distribution onto the M_{te} axis (c). The figures were published in Ref. [4].

EXPERIMENTS AT THE BEAM OF THE MT-25 IN FLNR (JINR)

The experiments dedicated to study of the (γ, *f*) reactions were performed at the beam of the MT-25 microtron in the Flerov Lab, using VEGA (V-E Guide based Array) setup. The scheme of the spectrometer is shown in figure 3(a).

Fission fragments (FFs) from the (γ, *f*) reaction in the target (1) is captured by the electrostatic guide system (EGS) consisted of the tube (2) and the central wire (3). The FF energy *E* and velocity *V* required for calculation of the FF mass are measured in the time-of-flight spectrometer consisted of the microchannel-plates based timing detector (4) and the mosaic of four PIN diodes (5).

Typical trajectories of the ions in the guide are shown in figure 3(b).

The EGS constitutes a cylindrical capacitor with a thin wire as a central electrode. Some fraction of the ions emitted from the target at one end of the guide can be involved in the spiral-like movement along the guide axis, thanks to the radial electric field, which suppresses the radial component of the ion velocity. According to [5], in which the EGS was proposed

for the first time, the collection efficiency F_c of the guide for an extended uniform target of radius *b* equal to the tube (outer cylinder) of radius *R*, is estimated to be:

$$F_c = {0.135qV_0}\Big/{\{E_n \ln({R}/{s})\}},$$

where V_0 is the potential difference between the two conductors, E_n is the kinetic energy of the fission fragment, s is the radius of the central wire of the guide, q is the ionic charge of the fragment.

Only minor part of the ions already caught in the guide will be lost along the flight pass, even if it is a very long one. Thus, the EGS allows it to increase a counting rate at the detector placed several meters away from the target.

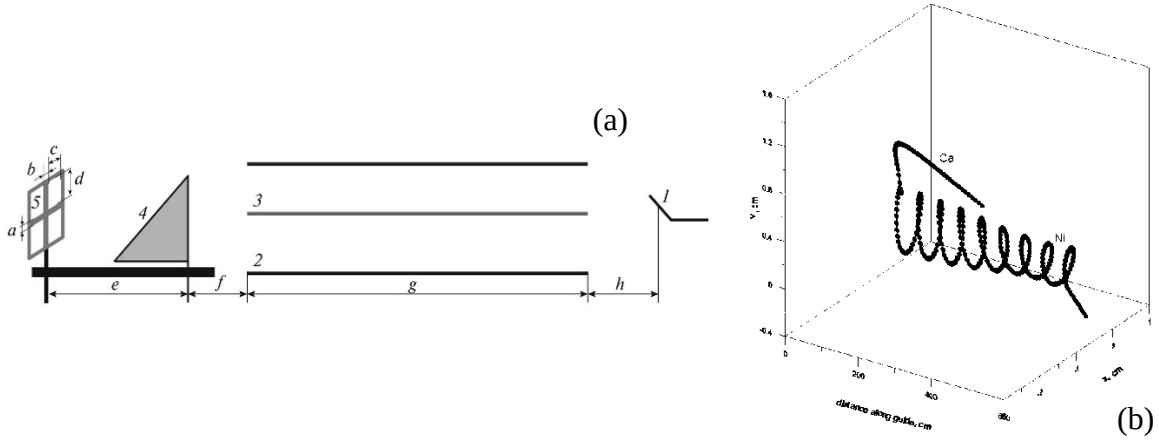

FIGURE 3. The scheme of the VEGA setup (a). A target of U isotope (1) is irradiated by the braking gamma quanta of the electron beam of the MT-25 microtron. Some fraction of the fission fragments is captured by the electrostatic guide system (EGS) consisting of a tube (2) at zero potential and the central wire (3) at a potential –10 kV. At the exit of the EGS, the FF energy *E* and velocity *V* for calculation of the FF mass are measured in the time-of-flight spectrometer consisting of the timing detector (4) and a mosaic of PIN diodes (5). The main dimensions of the setup: (*a*) vertical gap between the PIN diodes, 0.5 cm; (*b*) horizontal gap between the PIN diodes, 0.6 cm; (*c*) PIN diode's width, 1.8 cm; (*d*) PIN diode's length, 1.8 cm; (*e*) distance between the timing detector and the PIN diodes, 17.9 cm; (*f*) distance between the EGS and the timing detector, 3 cm; (*g*) EGS length, 400 cm; (*h*) distance between the target and the EGS, 3 cm. Typical trajectories of the ions in the guide (b).

The mass correlation distribution for the FFs from ^{235}U(γ, *f*) reaction detected in coincidence in two different PIN diodes of the mosaic is presented in figure 4(a).

Some linear structures inside the box w1 attract attention. This region is shown on a larger scale in figure 4(b). Solid lines 1–4 running at 45^0 to the M_1 axis match the expression $M_1 + M_2$ = const. Bottom two lines in figure 4(b) correspond to the missing masses 72 u and 68 u, respectively. These masses are associated with magic isotopes of ^{72}Ni and ^{68}Ni. As was shown in figure 1(b) just these really detected fragments manifested themselves as "Ni-bump".

The scheme in figure 4(c) illustrates a scenario standing behind the observables. The first rupture appears between the light fragment of Ni and heavy intermediate fragment of Gd. The letter undergoes a break-up in the foil of the timing detector. The delay between the first rupture and the break-up is about 400 ns to be the fragment time-of-flight of the electrostatic guide. The fact that there is a delay means that the Gd nucleus was born in the shape isomer state with the life-time exceeding 400 ns.

It should be stressed that a break-up of the *heavy* FF took place and both decay products were detected in *the same spectrometer arm*.

The mass-velocity distribution of the FFs from also the ^{235}U(γ, *f*) reaction for the FF multiplicity $m = 2$ is shown in figure 5(a). The FF multiplicity $m = 2$ means that two fragments with the masses M_1 and M_2 were detected in two different PIN diodes in coincidence. By definition, the FF masses of each event are indexed in such a way that $M_1 > M_2$. The locus of heavy fragments in the box *w*1 is shown in figure 5(b) in the larger scale. The projection of the distribution onto the mass axis is compared with the mass spectrum from conventional binary fission in figure 5(c). The spectra differ substantially due to two strong peaks corresponded to the masses 128 u and 134 u, respectively.

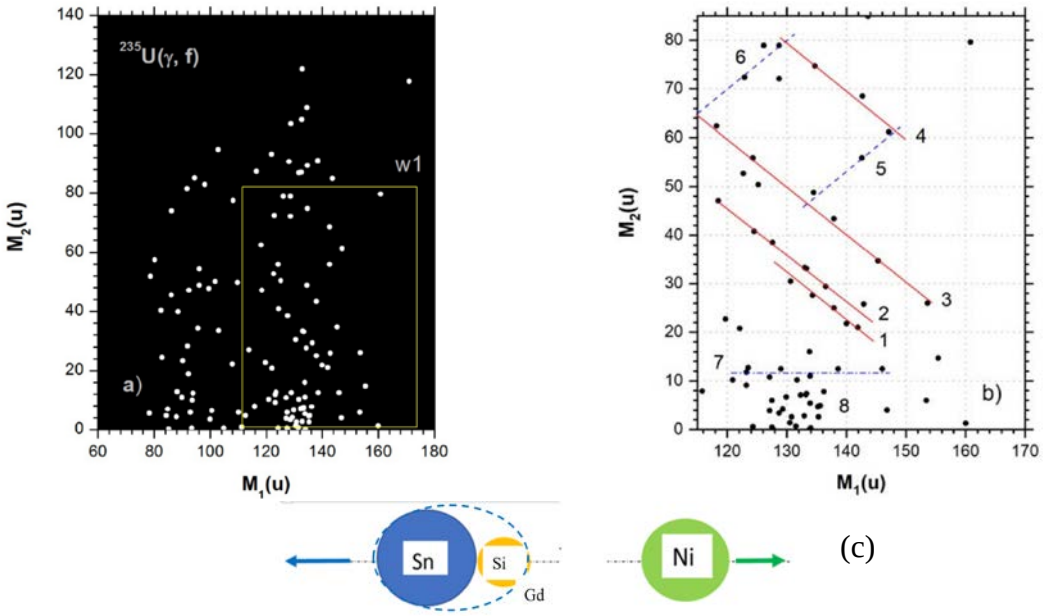

FIGURE 4. Mass correlation distribution for the FFs detected in coincidence in two different PIN diodes (a) and its part from box *w*1 (b). See text for details. The figures (a), (b) were published in Ref. [6].

And the last but not list – the spectrum in figure 5(c) agrees perfectly with the spectrum in figure 5(d) obtained at the LIS setup (see figure 2 (c)).

Thus, we observe similar result of the break-up of heavy FFs of two different mother systems in two different foils. Magic nuclei of ^{128}Sn and ^{134}Te demonstrate themselves as the cores of the deformed heavy fission fragments being in the shape isomer states.

The next figure 6 is dedicated to the ^{238}U(γ, *f*) reaction. The mass correlation distribution in figure 6(a) looks more complicated than in the previous reaction. Indeed, it includes not only the lines $M_1 + M_2 =$ const but also additional linear structures marked by the

arrows and vertical line at the mass 132 u in figure 6(b). The spectrum of the missing mass is shown in figure 6(c). Even the harshest referee could not deny the presence of at least a wide peak in the mass range (48–72) u. The same spectrum with 1 mass per channel is shown in figure 6(d).

The last one in the series of the targets studied so far was ^{232}Th (figure 7). We referred to the rhombic meander (figure 1(a)) in the introduction. As was shown by machine learning methods [8], the probability of a random realization of such a structure (rhombic meander) is negligible. Here, again, the lines $M_1 + M_2 = \text{const}$ and the lines $M_1 - M_2 = \text{const}$ are seen (figure 7). They perfectly describe the set of points that were obtained in this experiment. It should be noted that the ^{26}Ne fragment is seen both as detected and missing one. The points corresponded to the missing magic $^{46}Ar_{28}$ fragment is marked by the arrow.

The possible nature of the lines along which the sum of the masses is a constant, was discussed in our publication [9]. As for the structure $M_1 - M_2 = \text{const}$, its analysis is still in progress.

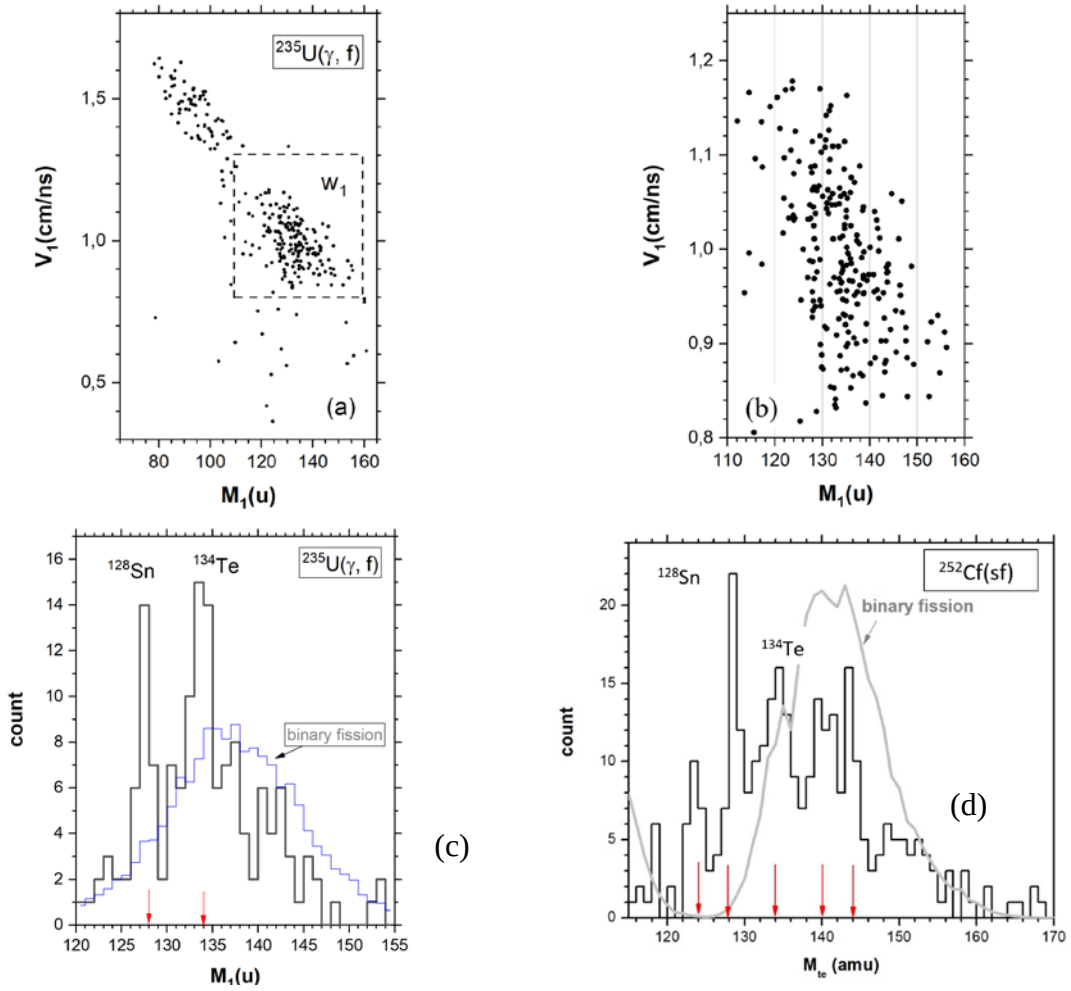

FIGURE 5. (a) – mass-velocity distribution of the heavy FFs from the ^{235}U(γ, *f*) reaction for the FF multiplicity $m = 2$; (b) – the distribution points from box *w*1 in figure 5(a); (c) – FFs mass spectra: the black one is a projection of the distribution in figure 5(b) on the axis M_1, the grey one is a mass spectrum for the FF's multiplicity $m = 1$. Positions of the magic FFs are marked by the arrows; (d) – a spectrum from figure 2(c) presented here for comparison with figure 5(c). The figures (a), (b), (c) were published in Ref. [7].

The experiments that are presented became possible after difficult and lengthy methodical work. For all the signals in the spectrometer we record their digital copy. For this purpose, a fast multichannel flash ADC is used. The current value of the signal is fixed each 200 ps for a gate duration of 200 ns. The data processing is performed offline. Our approach to the data processing is presented in Ref. [10] and references therein.

The main problem that we encountered, which is common for experiments on MT, is the background noise from the accelerator. In order to select only "suitable" events the base-line is inspected during 20 ns before the signal and both mean value and variance of the base-line are calculated. If actual fluctuations of the base-line exceed the level $C+3\sigma$ the signal is rejected. Unfortunately, only 20% of full statistics remains after such a selection.

Summing up, it should be stressed that exclusively thanks to the special impulse shaping unusual for the "classical" amplitude spectrometry and off-line processing of the digital images of all the signals we succeeded in the experiments at the gamma-beam.

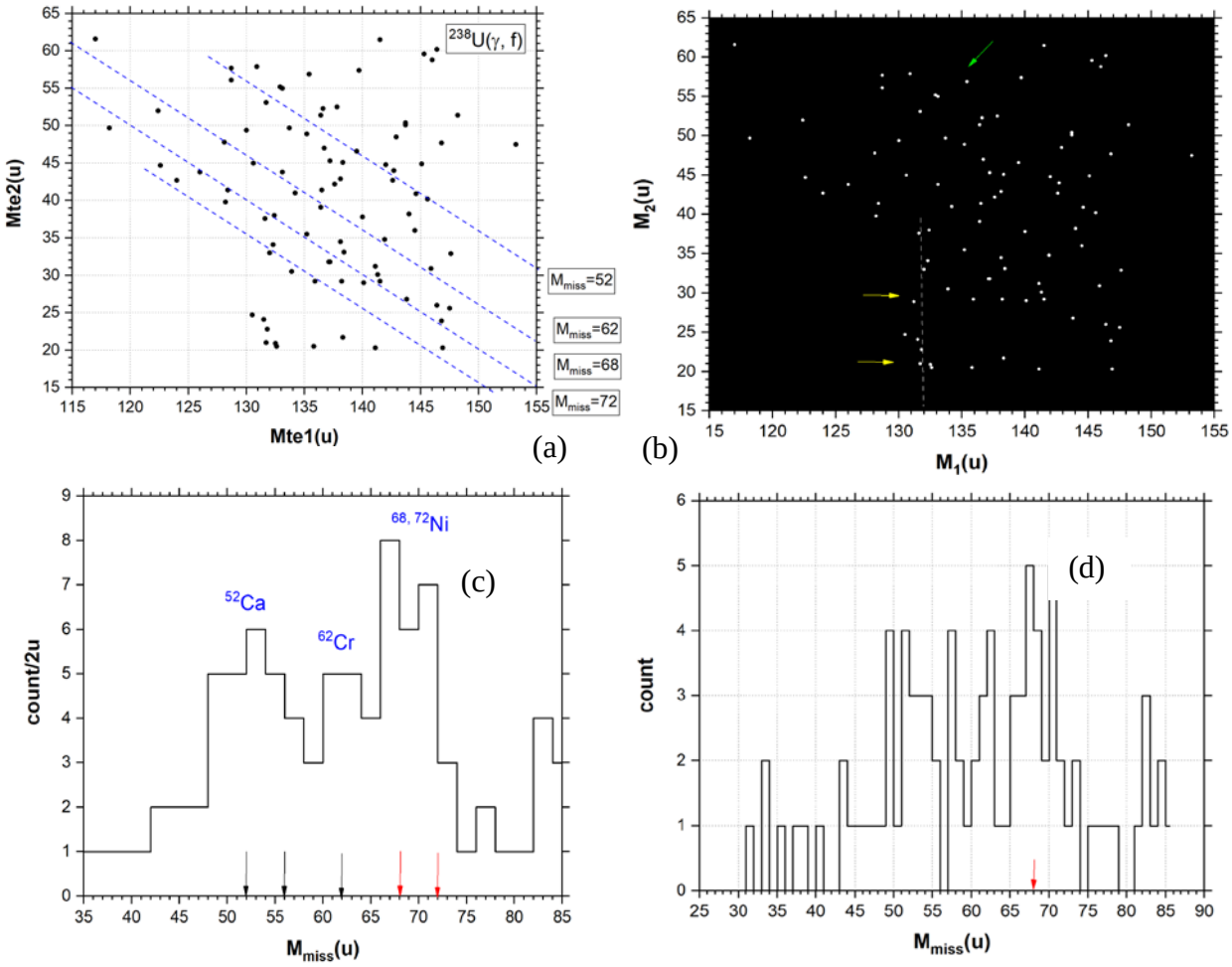

FIGURE 6. Mass correlation distribution for the FFs from the ^{238}U(γ, *f*) reaction detected in coincidence in two different PIN diodes (a), (b) and the spectrum of the missing mass M_{miss}= 238 – (M_1+M_2) for the same distribution (c), (d). The figures (a), (c) were published in Ref. [1].

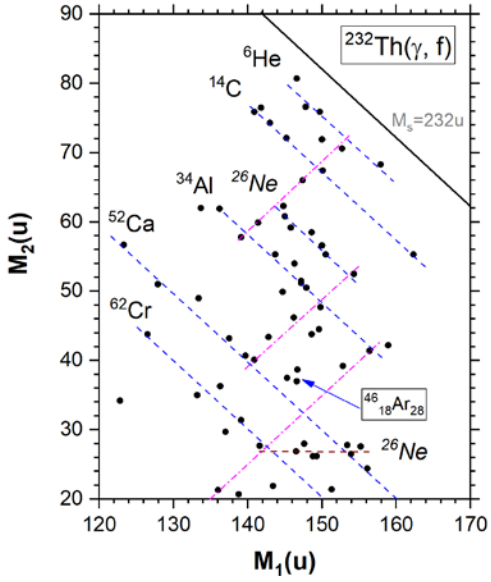

FIGURE 7. Mass correlation distribution for the FFs from the ^{232}Th(γ, *f*) reaction detected in coincidence in two different PIN diodes.

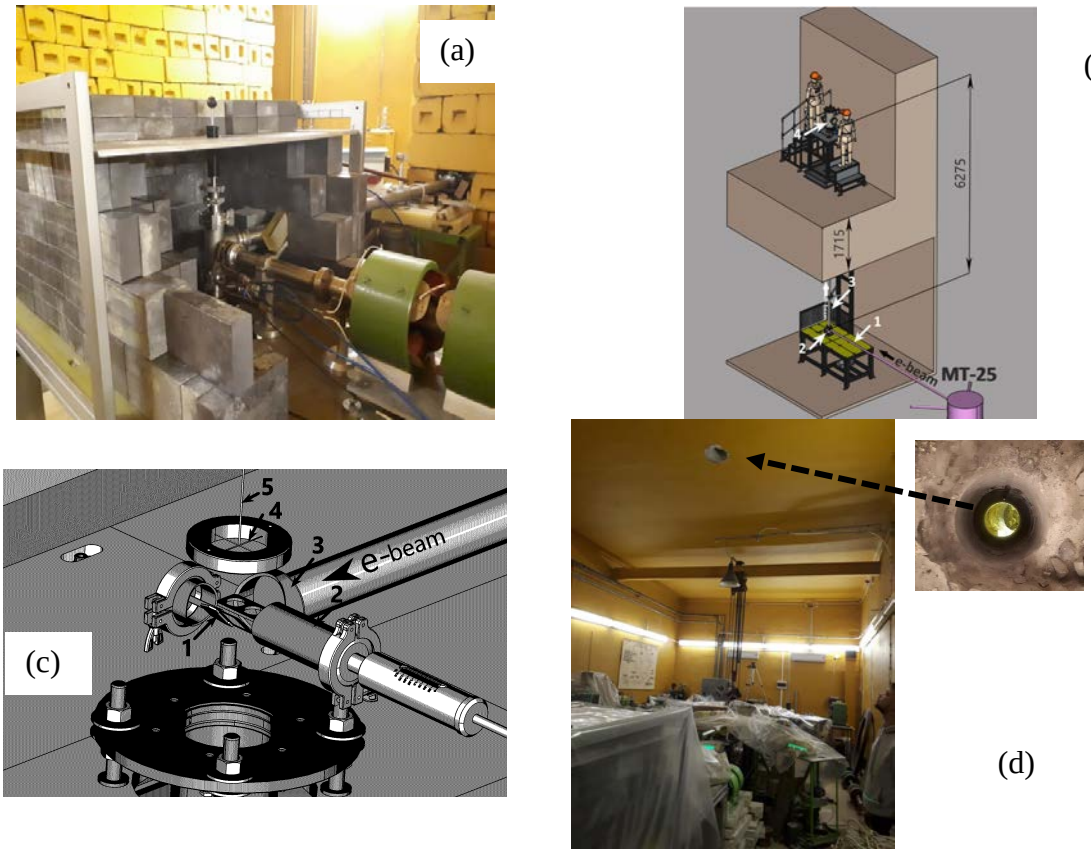

FIGURE 8. VEGA and VEGA-m setups. Target block of the VEGA setup in the lead shield (a). Schematical view of the VEGA-m setup (b): beam-line of the MT-25 microtrone (1), target block (2), EGS (3), detector chamber (4). Target holders and the bottom end of the EGS (c). Microtrone hall at the stage of drilling the concrete slab under the hall (d).

VEGA-M PROJECT

The main problem that was encountered, which is common for experiments on MT, is the background noise from the accelerator. Trivial but really ponderous way to protect the setup was already realized - significant time was spent to build a lead shield weighing several tons (figure 8(a)) what improved the experimental conditions but only partially.

To improve the situation radically, a new VEGA-m project is underway. The guide of about 6 meters long will now be positioned vertically and therefore enters the second floor of the microtron hall, passing about 2 *m* of concrete, which protects from radiation (figure 8(b)). Figure 8(c) shows the target holders and the bottom end of the EGS. Fortunately, one critical moment of the project is in the past: the stage of drilling the concrete slab has already been successfully completed (figure 8(d)) and a hole with a diameter of 220 mm for the new EGS is ready.

CONCLUSION

The following scenario could be proposed. Binary fission of the excited heavy nucleus occurs in the prescission configuration with the light magic fragment, for instance, Ni nucleus. The fragment is lost in the target backing, while the heavy fragment which is flying in the opposite direction is caught into EGS. After approximately *400 ns* ($<V_1> \approx 1$ cm/ns and the EGS length is about 400 cm) the heavy fragment reaches the start detector where its binary brake-up in very thin foil (50 μg/cm^2 of Al_2O_3) occurs. *The main conclusion which can be drawn from the result under discussion is that the heavy fragment of photo-fission of* ^{235,238}*U and* ^{232}*Th nuclei are born in the shape isomer states and the life time of these states exceeds 400 ns.* The result was obtained for the first time.

ACKNOWLEDGMENTS

The authors are grateful to V.I. Furman, Yu.M. Tchuvil'sky, G.G. Adamian, N.V. Antonenko, A.K. Nasirov for numerous fruitful discussions and stimulated criticism.

REFERENCES

1. D.V. Kamanina et al., Bull. Russ. Acad. Sci.: Phys. 87 (2023) 1238.
2. Yu.V. Pyatkov et al., Eur. Phys. J. A 45 (2010) 29.
3. Yu.V. Pyatkov et al., Eur. Phys. J. A 48, (2012) 94.
4. Yu.V. Pyatkov et al., Proceedings of the 23th International Seminar on Interaction of Neutrons with Nuclei, Dubna, Russia, 25-29 May 2015. Dubna 2016, p. 97–101.
5. N.C. Oakey, P.D. McFarlane, NIM 49 (1967) 220.
6. Yu.V. Pyatkov et al., Proceedings of the 27th International Seminar on Interaction of Neutrons with Nuclei, Dubna, Russia, 10-14 June 2019. Dubna 2020, p. 249–252.
7. Yu.V. Pyatkov et al., Physics of Atomic Nuclei 85 (2022) 292.
8. G. A. Ososkov et al., Phys. Part. Nucl. Lett. 18 (2021) 559.
9. Yu.V. Pyatkov et al., Eur. J. Phys. Funct. Mat. 4 (2020) 13.
10. Yu.V. Pyatkov et al., Bull. Russ. Acad. Sci.: Phys. 82 (2018) 804.